Stiffness-dependent intracellular location of cylindrical polymer brushes

*Antoine Niederberger, Théophile Pelras, Livia Salvati Manni, Paul A. FitzGerald, Gregory G. Warr and Markus Müllner**

Antoine Niederberger, Dr. Théophile Pelras, Dr. Livia Salvati Manni, Dr. Paul A. FitzGerald, Prof. Gregory G. Warr, Dr. Markus Müllner
Key Centre for Polymers and Colloids, School of Chemistry, The University of Sydney, Sydney, NSW 2006, Australia.
E-mail: markus.muellner@sydney.edu.au
Dr. Théophile Pelras, Prof. Gregory G. Warr, Dr. Markus Müllner
The University of Sydney Nano Institute (Sydney Nano), The University of Sydney, Sydney, NSW 2006, Australia.
Dr. Paul A. FitzGerald
Sydney Analytical, The University of Sydney, Sydney, NSW 2006, Australia

Keywords: molecular polymer brushes, polymer bottlebrushes, polymer nanoparticles, stiffness, cellular interactions

ABSTRACT: Cylindrical polymer brushes (CPBs) are macromolecules with nanoparticle proportions. Their modular synthesis enables tailoring of their chemical composition as well as the dialing-up of overall dimensions and physicochemical properties. In this study, we synthesized two rod-like poly[(ethylene glycol) methyl ether methacrylate] (PEGMA)-based CPBs with varying stiffness but otherwise comparable features and functionality. Differences in particle stiffness were assessed using small angle neutron scattering (SANS). We observed that the fate of our two CPBs within cells was distinctly different. Stiffer CPBs seem to gravitate towards the mitochondria, whereas CPBs with reduced stiffness were present in different intracellular vesicles.

1. Introduction

Nanoparticle-based delivery systems are being developed to tackle limitations of traditional delivery strategies for therapeutics and imaging diagnostics.[1–3] Especially polymeric nanoparticles can be custom-made to aid the detection, diagnosis and treatment of various illnesses.[4] Nanoscale polymer particles offer benefits to *in vivo* performance, such as protecting

drugs from early degradation, controlling drug release, improving circulation time, providing distinct biodistribution profiles as well as offering opportunities for passive and active targeting.[5] Particle size and surface chemsitry, in particular, have been linked to the overall nanoparticle behaviour in biologiocal domains.[6] A more recent focus on particle characteristics highlighted that there are more key parameters governing nanoparticle behaviour, with drug loading, shape and stiffness being considered additonal determinants.[7–12] The development of structure-function-property relationships is therefore becoming increasingly necessary, as more and more complex and multifunctional particle systems are developed.[13] Closer investigation of nanoparticle shape revealed its importance on particle interaction and transport in cell tissues and tumours. Especially cylindrical nanoparticles have repeatedly shown potential to match or outperform spherical analogues.[14–16] In this context, particle stiffness or elasticity is studied to a lesser content;[17–19] mostlikely also due to the difficulty of directly measuring and comparing differences in various particles systems. However, in general stiffer/harder nanoparticles exhibit shorter circulation times compared to their softer counterparts, and cells internalise stiffer nanoparticles at faster rates.[20,21] Computational studies of membrane interaction with soft and hard nanoparticles showed that harder particles are internalised more easily, with harder particles causing lesser deformation of the membrane and themselves being distorted minimally throughout the process compared to the softer counterparts.[22] However, *in vivo* studies suggest that stiffer particles can be readily internalised by macrophages, resulting in a shortening of their circulation times.[23] A conclusion on the effects of stiffness in cellular interactions, especially on the ideal stiffness, cannot yet be drawn conclusively.[24] However, systems that allow for fine-tuning stiffness as a key design parameter are gaining increasing attention, as the importance of mechanical properties of nanoparticles is increasingly unravelled.[5,17,20,24–27]

Polymer systems that offer syntheses of uniform nanoparticles, including control over key parameters, such as those described previously, are necessary to further develop polymer nanomedicines. In this context, nanoparticles based on cylindrical polymer brushes (CPBs) are

increasingly being studied.[28–31] CPBs consist of a polymeric backbone that is grafted with shorter side chains. Side chain crowding and their steric hindrance results in the stretching of the backbone, and the CPBs adopt a rod-like conformation.[32] CPBs avoid the interchain entanglement observed in solutions of linear polymers,[32,33] and effectively form unimolecular particulates.[34,35] There are three main ways to obtain CPBs using well-established grafting strategies.[36] They allow systematic and independent variation of parameters such as size (backbone and side chains), shape (by varying backbone length) and key physicochemical properties (surface chemistry, heterogenity). Thus, CPBs are nanoparticle systems that should allow a more direct comparison as parameters can be altered independently.

In this study, we designed two CPBs with comparable size, shape and surface chemistry, but distinctly different stiffness. Specifically, hydrophilic CPBs with side chains of poly[(ethylene glycol) methy ether methacrylate] (PEGMA) and glycidyl methacrylate (GMA) were synthesised. One of the brushes was equipped with an additional hydrophobic core of n-butyl methacrylate (nBMA) to modulate the stiffness of the brush along its core (Figure 1). The overall size, shape and chemical composition was assessed using proton nuclear magnetic resonance (^{1}H NMR) and atomic force microscopy (AFM). The difference in stiffness between the two CPBs was determined by small angle neutron scattering (SANS). Finally, the CPBs behaviour with two different cancer cell types was compared *in vitro*.

Rod-like CPBs were obtained using a polyinitiator backbone consisting of poly(2-(2-bromoisobutyryloxy)ethyl methacrylate) (PBIEM) with a relatively high degree of polymerisation (DP = 2700). Its synthesis is a combination of anionic polymerization and post-polymerization modifications and has been detailed in previous studies.[37–39] Using atom transfer radical polymerisation (ATRP) and grafting-from approach, we produced two different CPBs each containing copolymers side chains of PEGMA and GMA (5 mol%), with one brush featuring an additional short block of P*n*BMA as a core (Figure 1, Supporting Information S1). We anticipated that the higher glass transition temperature of the core ($T_{g,PnBMA}$ = 20 °C) in one

of the CPBs would increase its stiffness compared to the core-lacking CPBs analogue, while keeping the overall dimensions and surface chemistry comparable. The presence of GMA in the CPBs enabled the subsequent attachment of fluorescent dyes (Atto 633) via 'click' chemistry using our previously established protocol.[31]

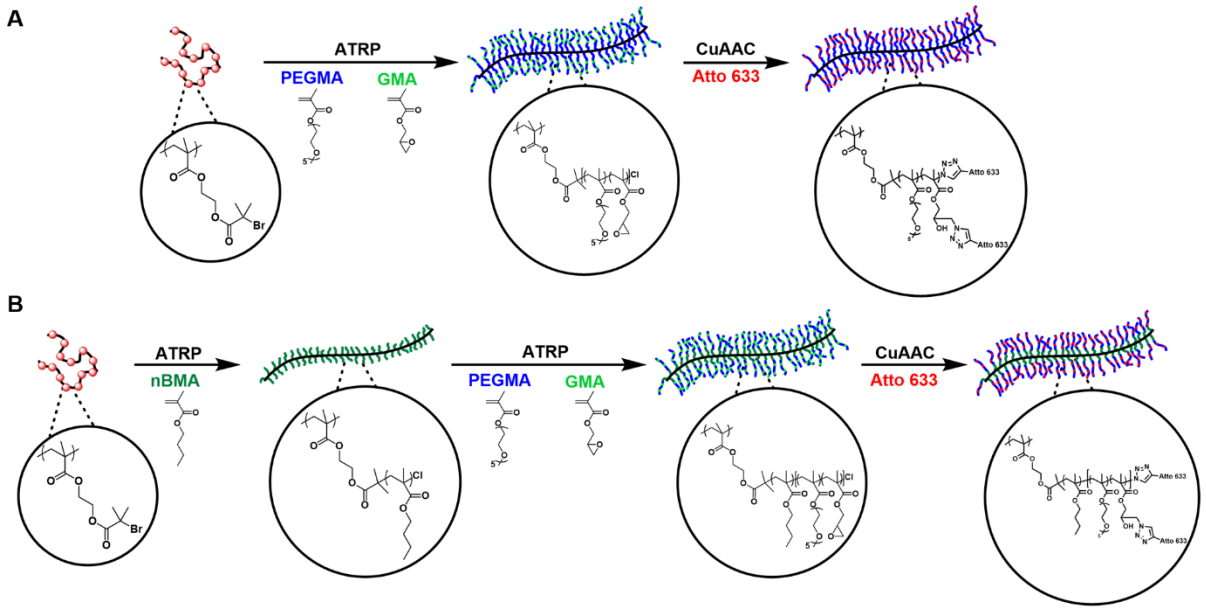

Figure 1. Schematic representation of the synthesis process for PBIEM$_{1350}$-co-[(PEGMA$_{123}$-co-GMA$_7$)]$_{1350}$ CPB (A) and PBIEM$_{1350}$-co-[*n*BMA$_{15}$-b-(PEGMA$_{114}$-co-GMA$_6$)]$_{1350}$ CPB (B).

We established the chemical composition of our CPBs using proton nuclear magnetic resonance (^{1}H NMR) (Supporting Information S2). Using standard protocols for CPBs, we used the monomer conversion, and previously reported grafting efficiencies from PBIEM backbones,[40,41] to calculate the overall composition of our CPBs: namely, PBIEM$_{1350}$-co-[(PEGMA$_{123}$-co-GMA$_7$)]$_{1350}$ (for the core-lacking CPB) and PBIEM$_{1350}$-co-[nBMA$_{15}$-b-(PEGMA$_{114}$-co-GMA$_6$)]$_{1350}$ (for the core-containing CPB). These CPBs were then modified using sodium azide and 'clicked' with alkyne containing Atto 633 dyes. Fluorescence spectroscopy analysis of the dye modified CPBs in water verified the successful incorporation of fluorescent probes. Both brushes exhibited the expected emission peak at 651 nm (Supporting Information S3).

The cylindrical shape of the brushes was verified by tapping-mode atomic force microscopy (AFM) on freshly cleaved mica (Figure 2A-D, Supporting Information S4). Both CPBs showed the expected rod-like morphology and showed minimal aggregation. CPBs typically flatten on substrates during drying, resulting in the side chains spreading and a decrease in height to only a few nm. Both our CPBs showed similar heights of 3-5nm, while the average length and width of the brushes was between 200-250 nm and 40-50 nm, respectively. This correlated well with a previous study using the same polymer backbone.[42] Similarly, some scission was observed due to strong forces acting on the brushes during the deposition and drying process.[40,43]

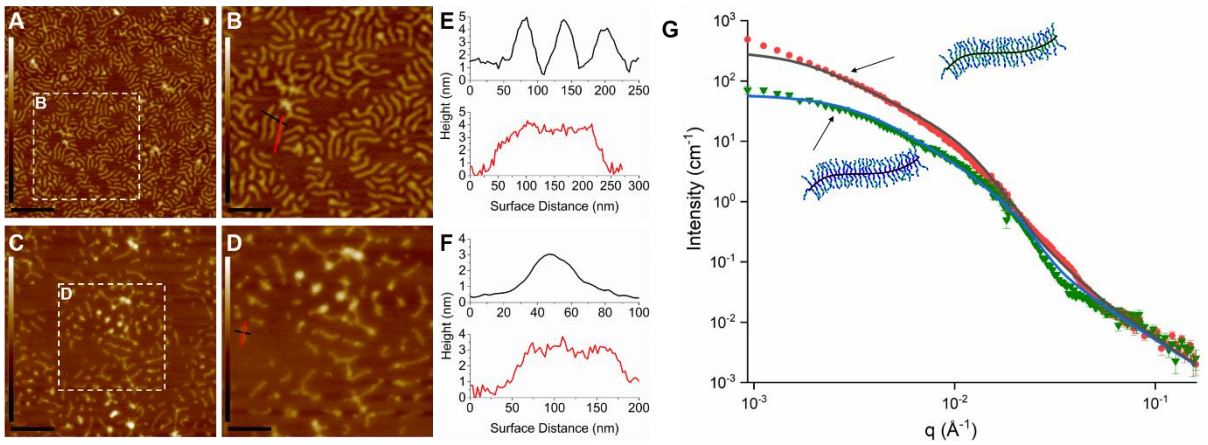

Figure 2. AFM height images of (A/B) PBIEM$_{1350}$-co-[(PEGMA$_{123}$-co-GMA$_7$)]$_{1350}$ and (C/D) PBIEM$_{1350}$-co-[nBMA$_{15}$-b-(PEGMA$_{114}$-co-GMA$_6$)]$_{1350}$ spin-coated onto freshly cleaved mica from acetone solution (0.2 g.L^{-1}). Cross-sectional analyses (E) and (F) extracted from (B) and (D) respectively. Scale bars are 1 µm (A/C) and 600 nm (C/D), z-scale is 20 nm. (G) SANS pattern of PBIEM$_{1350}$-co-[(PEGMA$_{123}$-co-GMA$_7$)]$_{1350}$ (green triangles) and PBIEM$_{1350}$-co-[nBMA$_{15}$-b-(PEGMA$_{114}$-co-GMA$_6$)]$_{1350}$ (red circles), fitted with flexible cylinders and blobs (solid lines) with Kuhn lengths of 236 Å and 906 Å, respectively. Data was collected at 25°C in D_2O and backgrounds have been subtracted.

To characterize the relative stiffness of the two CPBs in an aqueous environment, we employed small angle neutron scattering (SANS). SANS patterns (Figure 2G) were fitted with a flexible cylinder model combined with blobs for both CPBs. All obtained parameters of the fit are comparable for the two systems (see Supporting Information, Tables S1 and S2). Small differences in the radius and in the scattering length density (SLD) of the two CPBs are expected due to the different hydrophilicity of the side chains. The relative stiffness of the two CPBs was determined by the fit value of the Kuhn length. The $PBIEM_{1350}$-co-[*n*BMA_{15}-b-($PEGMA_{114}$-co-GMA_6)]$_{1350}$ CPBs have a Kuhn length almost 4 times higher than the $PBIEM_{1350}$-co-[($PEGMA_{123}$-co-GMA_7)]$_{1350}$ CPBs, indicating much greater stiffness when the short P*n*BMA core is present. We hypothesize that although the P*n*BMA core chains are relatively short, they would introduce significant steric constraints, which in turn leads to a stiffening of the overall CPB along the backbone. SANS also provided information about the conformation of the CPBs in solution. In our case, the CPBs adopted a conformation of elastic cylinders, underscoring our AFM analysis. Given their similar morphology and that their chemical composition was predominately PEGMA, we treated the CPBs as structural and chemical analogues (*i.e.* comparable in size, shape and chemical identity), with the main difference being their stiffness (stemming from the PnBMA core, which had a DP of 15 and equated to roughly 5% of the overall CPB molecular weight).

Next, we sought to investigate the effect of this stiffness variation on cancer cells. Using MTT assays, we firstly studied the cytocompatibility of our two CPB systems on DLD-1 colorectal adenocarcinoma and A549 adenocarcinomic alveolar basal epithelial cell lines, respectively. Over various concentration (0.02-1.0 $g.L^{-1}$) both CPBs were compatible with either cell line (Supporting Information S5). Next, we assessed the effect of stiffness on intracellular location via confocal laser scanning microscopy (CLSM). We incubated the CPBs (0.2 $g.L^{-1}$) with DLD-1 and A549 cells for 24h before imaging (Figure 3). Without the PnBMA core, the ‘softer’ CPBs appear to be localized within vesicular compartments (likely

endosomes) for both cell lines. However, stiffer CPBs seem to be predominately localized in the mitochondria – again in either cell line.

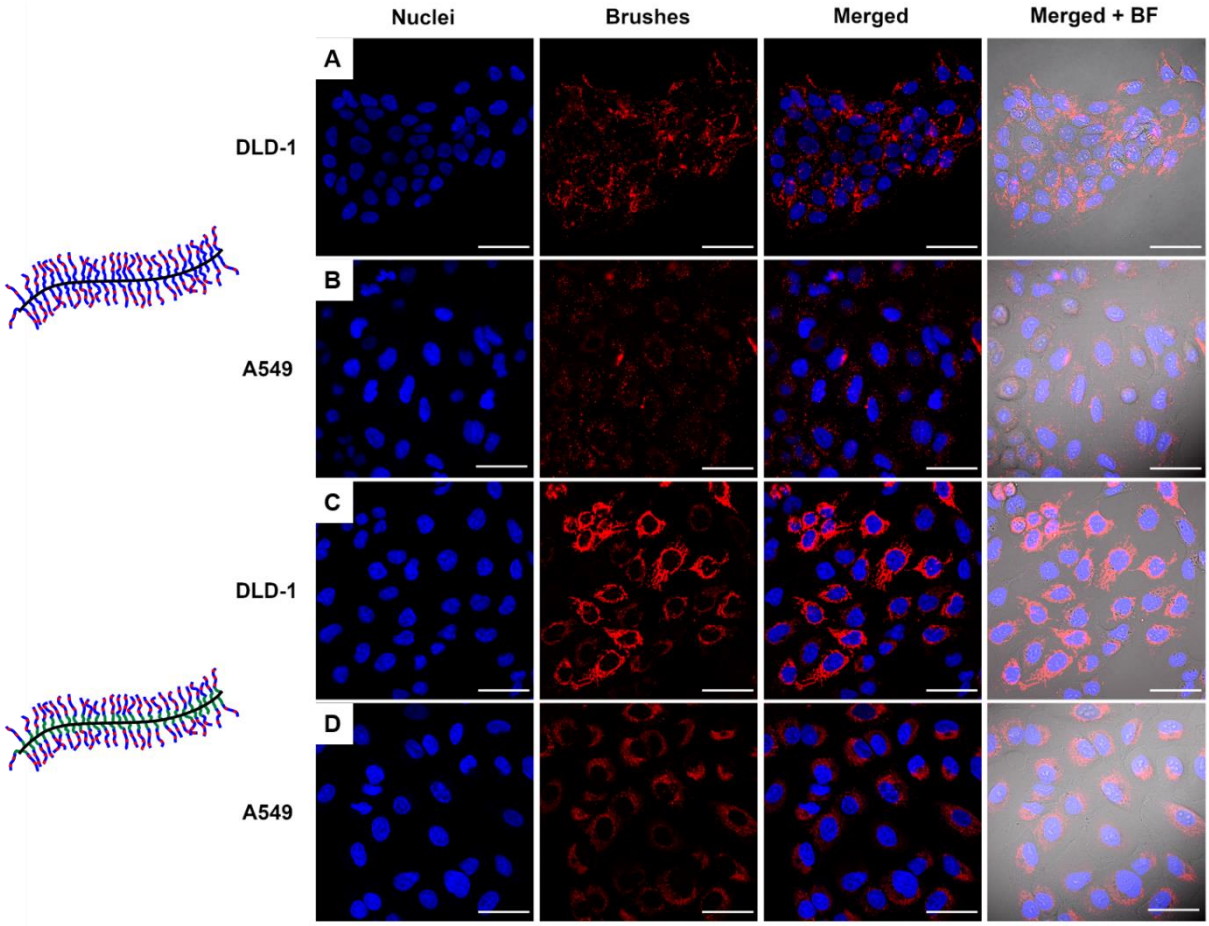

Figure 3. Confocal laser scanning microscopy (CLSM) images of PBIEM$_{1350}$-co-[(PEGMA$_{123}$-co-GMA$_7$)]$_{1350}$ incubated with (A) DLD-1 (A) and (B) A549 cells. PBIEM$_{1350}$-co-[nBMA$_{15}$-b-(PEGMA$_{114}$-co-GMA$_6$)]$_{1350}$ incubated with (C) DLD-1 and (D) A549 cells. Scale bars are 50 µm. Each row shows (from left to right): nuclei, CPBs, nuclei+CPB, and nuclei+CPBs+bright field. Colour code: blue (Hoechst 33342) = cell nuclei; red (Atto 633) = CPBs.

To further investigate our hypothesis of stiffer CPBs being located inside the mitochondria, we co-incubated the cells with a 50nM solution of MitoTracker Green (Figure 4) and LysoTracker Green (Figure S6). Our co-localisation study confirmed that the stiffer CPBs are indeed associated with the mitochondria (Pearson's coefficient R = 0.75) as further demonstrated by the overlapping fluorescence of brushes (red) and mitotracker (green) (Figure

4, merged channel, Supporting Information S6). The experiment further highlighted that the CPBs without a core (*i.e.* the more flexible CPBs) had minimal overlap with the Mitotracker location (R = 0.14). Recent studies have shown the effect of fluorescent dyes on the location of nanomaterials (e.g. positively charged Atto dyes can be used for mitochondria imaging[44]). Kempe and co-worker recently found that Cy5-labeled polymers can passively diffuse the cell membrane to target mitochondria,[45] and that the intracellular fate depends on the type of Cy5 dye used.[46] However, in our case, both CPBs systems have been modified with the same dyes and no noticeable charge was introduced to the CPBs as measured by ζ-potential (both around -0.1mV). Consequently, the different behaviour must be attributed to the difference in mechanical properties which may result in activating different internalization pathways. This is further corroborated by comparing cell-normalized intracellular fluorescence intensities in Figure 3, which indicated stiffer brushes associated nearly twice as much with cells compared to their softer counterparts (despite the stiffer brushes exhibiting a slightly lower normalized fluorescence than the softer ones; Supporting Information S3). We are keen to explore this phenomenon in detailed biological studies.

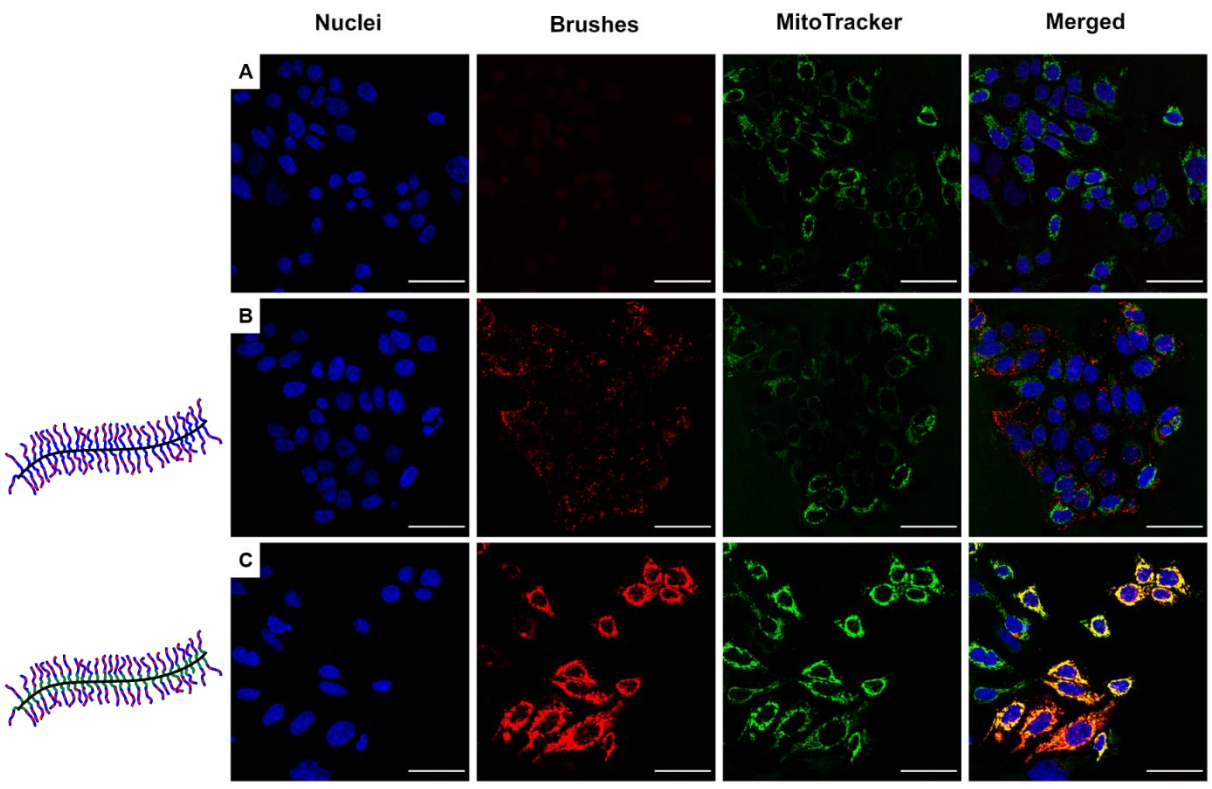

Figure 4. CLSM images of A549 cells. (A) Control (i.e. no brushes present), (B) $PBIEM_{1350}$-co-$[(PEGMA_{123}$-co-$GMA_7)]_{1350}$ and (C) $PBIEM_{1350}$-co-$[nBMA_{15}$-b-$(PEGMA_{114}$-co-$GMA_6)]_{1350}$ brushes. Each row shows (from left to right): nuclei, CPBs, Mitotracker, and nuclei+CPBs+Mitotracker. Scale bars are 50 µm. Color code: blue (Hoechst 33342) = cell nuclei; red (Atto 633) = CPBs; green (Mitotracker green) = mitochondria.

In conclusion, CPBs offer a straightforward strategy to develop tailor made polymeric nanoparticles in which multiple parameters can be altered independently to study nanoparticle behaviour with cells. In particular, we could use CPBs to reveal the impact of stiffness changes to the intracellular location of polymer nanorods. Specifically, we produced two CPB systems, predominately containing PEGMA and comparable in size, shape, and surface chemistry, and introduced stiffness changes via the addition of a hydrophobic core. The addition of the core significantly altered the Kuhn length of the CPB, increasing it by a factor of 4 when compared to the core-lacking counterpart. These differences accessed by SANS ultimately proved significant in the way the CPBs interact with cancer cells, where the stiffer CPBs would end up in the mitochondria while the 'softer' CPBs were exclusively localized in other compartments in the cytoplasm. Studies are ongoing to further investigate this peculiar behaviour. However, our study highlights the potential of CPBs as designer nanomaterials to study, and tailor, the behaviour of polymer nanoparticles for nanomedicine applications (e.g., targeting towards specific organelles).

Supporting Information

Supporting Information is available from the Wiley Online Library or from the author.

Acknowledgements

The authors greatly acknowledge the free use of SasView (http://www.sasview.org/), developed under the NSF award DMR-0520547, SINE2020 project, grant agreement No 654000. The

authors thank Prof. Chiara Neto for providing access to atomic force microscopes and the Key Centre for Polymers and Colloids (KCPC) for access to equipment. T.P. was a grateful recipient of a Sydney Nano Postgraduate Top-Up Scholarship. T.P., P.F., G.G.W and M.M. thank the Australian Nuclear Science and Technology Organization (ANSTO, P5694) for beam line access on Quokka. M.M. acknowledges the Australian Research Council (DE180100007, FT200100185) for support. This project was funded through an ARC DECRA (DE180100007).

Received: ((will be filled in by the editorial staff))
Revised: ((will be filled in by the editorial staff))
Published online: ((will be filled in by the editorial staff))

References

1 A. G. Arranja, V. Pathak, T. Lammers and Y. Shi, *Pharmacol. Res.*, 2017, **115**, 87–95.

2 M. J. Mitchell, M. M. Billingsley, R. M. Haley, M. E. Wechsler, N. A. Peppas and R. Langer, *Nat. Rev. Drug Discov.*, 2021, **20**, 101–124.

3 M. W. Tibbitt, J. E. Dahlman and R. Langer, *J. Am. Chem. Soc.*, 2016, **138**, 704–717.

4 J. H. Park, S. Lee, J.-H. Kim, K. Park, K. Kim and I. C. Kwon, *Prog. Polym. Sci.*, 2008, **33**, 113–137.

5 A. C. Anselmo and S. Mitragotri, *Bioeng. Transl. Med.*, 2016, **1**, 10–29.

6 M. Elsabahy and K. L. Wooley, *Chem. Soc. Rev.*, 2012, **41**, 2885.

7 M. Longmire, P. L. Choyke and H. Kobayashi, *Nanomedicine*, 2008, **3**, 703–717.

8 S. M. Moghimi, A. C. Hunter and J. C. Murray, *Pharmacol. Rev.*, 2001, **53**, 283–318.

9 P. Decuzzi, B. Godin, T. Tanaka, S.-Y. Lee, C. Chiappini, X. Liu and M. Ferrari, *J. Control. Release*, 2010, **141**, 320–327.

10 M. Müllner, D. Mehta, C. J. Nowell and C. J. H. Porter, *Chem. Commun.*, 2016, **52**, 9121–9124.

11 M. H. Stenzel, *Angew. Chemie Int. Ed.*, 2021, **60**, 2202–2206.

12 M. Callari, P. L. De Souza, A. Rawal and M. H. Stenzel, *Angew. Chemie Int. Ed.*,

2017, **56**, 8441–8445.

13 M. Nowak, T. D. Brown, A. Graham, M. E. Helgeson and S. Mitragotri, *Bioeng. Transl. Med.*, 2020, **5**, e10153.

14 M. Müllner, K. Yang, A. Kaur and E. J. New, *Polym. Chem.*, 2018, **9**, 3461–3465.

15 Y. Tsukahara, S. Namba, J. Iwasa, Y. Nakano, K. Kaeriyama and M. Takahashi, *Macromolecules*, 2001, **34**, 2624–2629.

16 Y. Geng, P. Dalhaimer, S. Cai, R. Tsai, M. Tewari, T. Minko and D. E. Discher, *Nat. Nanotechnol.*, 2007, **2**, 249–255.

17 A. C. Anselmo and S. Mitragotri, *Adv. Drug Deliv. Rev.*, 2017, **108**, 51–67.

18 Y. Hui, X. Yi, D. Wibowo, G. Yang, A. P. J. Middelberg, H. Gao and C.-X. Zhao, *Sci. Adv.*, 2020, **6**, eaaz4316.

19 Y. Zheng, L. Xing, L. Chen, R. Zhou, J. Wu, X. Zhu, L. Li, Y. Xiang, R. Wu, L. Zhang and Y. Huang, *Biomaterials*, 2020, **262**, 120323.

20 A. C. Anselmo, M. Zhang, S. Kumar, D. R. Vogus, S. Menegatti, M. E. Helgeson and S. Mitragotri, *ACS Nano*, 2015, **9**, 3169–3177.

21 M. Yu, L. Xu, F. Tian, Q. Su, N. Zheng, Y. Yang, J. Wang, A. Wang, C. Zhu, S. Guo, X. Zhang, Y. Gan, X. Shi and H. Gao, *Nat. Commun.*, 2018, **9**, 2607.

22 J. Sun, L. Zhang, J. Wang, Q. Feng, D. Liu, Q. Yin, D. Xu, Y. Wei, B. Ding, X. Shi and X. Jiang, *Adv. Mater.*, 2015, **27**, 1402–1407.

23 J. Key, A. L. Palange, F. Gentile, S. Aryal, C. Stigliano, D. Di Mascolo, E. De Rosa, M. Cho, Y. Lee, J. Singh and P. Decuzzi, *ACS Nano*, 2015, **9**, 11628–11641.

24 Z. Li, C. Xiao, T. Yong, Z. Li, L. Gan and X. Yang, *Chem. Soc. Rev.*, 2020, **49**, 2273–2290.

25 T. D. Brown, N. Habibi, D. Wu, J. Lahann and S. Mitragotri, *ACS Biomater. Sci. Eng.*, 2020, **6**, 4916–4928.

26 J. Zhao, H. Lu, Y. Yao, S. Ganda and M. H. Stenzel, *J. Mater. Chem. B*, 2018, **6**,

4223–4231.

27 A. Garapaty and J. A. Champion, *Bioeng. Transl. Med.*, 2017, **2**, 92–101.

28 M. Müllner, *Macromol. Chem. Phys.*, 2016, **217**, 2209–2222.

29 T. Pelras, C. S. Mahon and M. Müllner, *Angew. Chemie Int. Ed.*, 2018, **57**, 6982–6994.

30 H. Li, H. Liu, T. Nie, Y. Chen, Z. Wang, H. Huang, L. Liu and Y. Chen, *Biomaterials*, 2018, **178**, 620–629.

31 M. Müllner, S. J. Dodds, T.-H. Nguyen, D. Senyschyn, C. J. H. Porter, B. J. Boyd and F. Caruso, *ACS Nano*, 2015, **9** (2), 1294-1304.

32 S. S. Sheiko, B. S. Sumerlin and K. Matyjaszewski, *Prog. Polym. Sci.*, 2008, **33**, 759–785.

33 M. Wintermantel, M. Gerle, K. Fischer, M. Schmidt, I. Wataoka, H. Urakawa, K. Kajiwara and Y. Tsukahara, *Macromolecules*, 1996, **29**, 978–983.

34 Y. Tsukahara, S. Namba, J. Iwasa, Y. Nakano, K. Kaeriyama and M. Takahashi, *Macromolecules*, 2001, **34**, 2624–2629.

35 M. Müllner and A. H. E. Müller, *Polymer*, 2016, **98**, 389–401.

36 M. Zhang and A. H. E. Müller, *J. Polym. Sci. Part A Polym. Chem.*, 2005, **43**, 3461–3481.

37 M. Zhang, T. Breiner, H. Mori and A. H. E. Müller, *Polymer*, 2003, **44**, 1449–1458.

38 M. Müllner, T. Lunkenbein, J. Breu, F. Caruso and A. Mueller, *Chem. Mater.*, **24**, 1802–1810.

39 M. Müllner, T. Lunkenbein, M. Schieder, A. Gröschel, N. Miyajima, M. Förtsch, J. Breu, F. Caruso and A. Mueller, *Macromolecules*, **45**, 6981–6988.

40 Z. Zheng, M. Müllner, J. Ling and A.H.E. Müller, *ACS Nano*, **7**, 2284–2291.

41 D. Neugebauer, B. S. Sumerlin, K. Matyjaszewski, B. Goodhart and S. S. Sheiko, *Polymer*, 2004, **45**, 8173–8179.

42 T. Pelras, H. T. T. Duong, B. J. Kim, B. S. Hawkett and M. Müllner, *Polymer*, 2017,

112, 244–251.

43 I. Park, A. Nese, J. Pietrasik, K. Matyjaszewski and S. S. Sheiko, *J. Mater. Chem.*, 2011, **21**, 8448.

44 Y. Han, M. Li, F. Qiu, M. Zhang and Y.-H. Zhang, *Nat. Commun.*, 2017, **8**, 1307.

45 A. M. Mahmoud, P. A. J. M. de Jongh, S. Briere, M. Chen, C. J. Nowell, A. P. R. Johnston, T. P. Davis, D. M. Haddleton and K. Kempe, *ACS Appl. Mater. Interfaces*, 2019, **11**, 31302–31310.

46 A. M. Mahmoud, J. P. Morrow, D. Pizzi, A. M. Azizah, T. P. Davis, R. F. Tabor and K. Kempe, *Biomacromolecules*, 2020, **21**, 3007–3016.

Cylindrical polymer brushes can be synthesized to exhibit different stiffness, while maintaining comparable dimensions and surface chemistry. Differences in stiffness translated into distinctly different behaviour *in vitro*, whereby stiffer brushes were localized in the mitochondria of cancer cells while their softer analogues were exclusively found in other compartments within the cytoplasm.

Antoine Niederberger, Théophile Pelras, Livia Salvati Manni, Paul A. FitzGerald, Gregory G. Warr and Markus Müllner*

Stiffness-dependent intracellular location of cylindrical polymer brushes